

# Node Masking: Making Graph Neural Networks Generalize and Scale Better

Pushkar Mishra<sup>1</sup> Aleksandra Piktus<sup>1</sup> Gerard Goossen<sup>2</sup> Fabrizio Silvestri<sup>1</sup>

## Abstract

Graph Neural Networks (GNNs) have received a lot of interest in the recent times. From the early *spectral* architectures that could only operate on undirected graphs per a *transductive* learning paradigm to the current state of the art *spatial* ones that can apply *inductively* to arbitrary graphs, GNNs have seen significant contributions from the research community. In this paper, we discuss some theoretical tools to better visualize the operations performed by state of the art spatial GNNs. We analyze the inner workings of these architectures and introduce a simple concept, *node masking*, that allows them to generalize and scale better. To empirically validate the theory, we perform several experiments on two widely used benchmark datasets for node classification in both transductive and inductive settings.

## 1. Introduction

Graphs are the most effective way of representing different types of entities and relationships amongst them. Several constructs inherently involve the notion of graphs, such as social networks, molecular structures, knowledge bases, recommendation systems, etc. Over the past few year, learning on graphs has become increasingly popular, applications of which can be found in domains ranging from abuse detection (Mishra et al., 2019) and document classification (Kipf & Welling, 2017) to knowledge graph alignment (Wang et al., 2018) and relation extraction in texts (Sahu et al., 2019). Learning on graphs is essentially about leveraging the inductive bias imposed by their relational structures, i.e., *relational inductive bias*, so as to achieve better performance on tasks that can benefit from relation reasoning (Battaglia et al., 2018). The ability to exploit relationships amongst entities in the data is a crucial one for advancing the state of AI (Tenenbaum et al., 2011; Lake & Baroni, 2017).

<sup>1</sup>Facebook AI, London, United Kingdom <sup>2</sup>Facebook, London, United Kingdom. Correspondence to: Pushkar Mishra <pushkarmishra@fb.com>.

A graph is defined by its set of nodes (i.e., vertices) and its set of edges. There exist two different paradigms for learning on graphs, *transductive* and *inductive*. In transductive learning, the nodes and edges remain constant across the training and prediction phases. In other words, at training time, the learning algorithm has access to all the nodes and edges including those for which predictions are to be made. Note that transductive paradigm does not support generalization to unseen nodes and edges. Figure 1 depicts node classification performed in transductive setting.

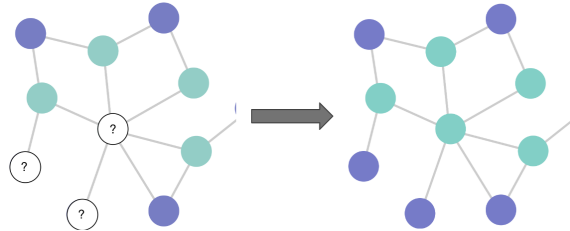


Figure 1. Node classification in transductive setting. At training time, the learning algorithm has access to all the nodes and edges including nodes for which labels are to be predicted.

In inductive learning, first a model  $\mathcal{H}$  is learned over the *training* graph consisting of some nodes and edges. The learned model is then used to predict on *unseen* nodes and edges that may or may not be disconnected from the nodes and edges in the training graph (Chiang et al., 2019). Note that some works (Veličković et al., 2018; Hamilton et al., 2017) have instead interpreted inductive learning to mean that the model is first trained on a set of graphs and then applied to a separate set of graphs. But the former interpretation subsumes the latter in that a set of graphs can be treated as a single graph with multiple disconnected components. Figure 2 depicts node classification in inductive setting.

Deep learning has brought advancements to several areas within AI. That said, deep learning on graphs is a rather challenging task to perform with traditional architectures like Convolutional Neural Networks or Recurrent Neural Networks. In the recent years, a lot of research has been dedicated to generalizing the convolution operation to graphs (Bruna et al., 2014; Kipf & Welling, 2017; Hamilton et al., 2017; Xu et al., 2019), which has formed the basis of all modern *graph neural networks* (GNNs). From the early *spectral* architectures that could only operate on undirected

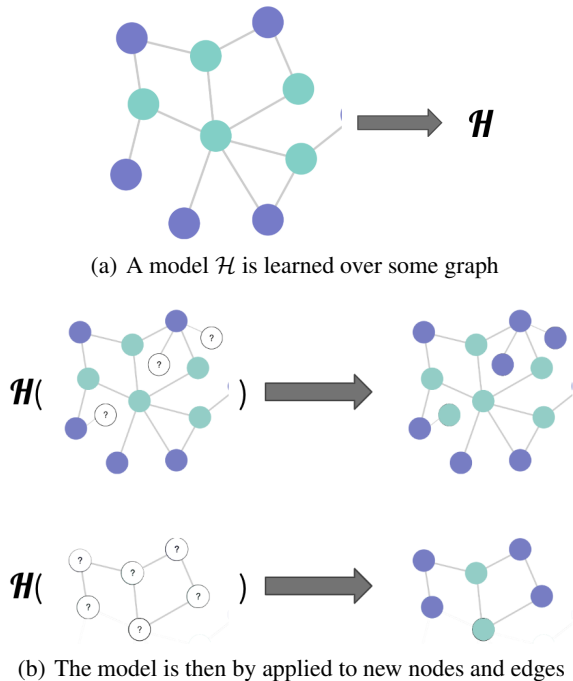


Figure 2. Node classification in inductive setting. Once learned, the model can be applied to new unseen nodes (outlined in red). There may or may not exist edges between such new nodes and the nodes used for training.

graphs in transductive settings to the current state of the art *spatial* ones that can apply *inductively* to arbitrary graphs, GNNs have undergone significant developments. This paper makes contributions towards further enhancing the capabilities of state of the art spatial GNNs.

**Our contributions.** We begin by discussing some theoretical tools to better visualize the operations performed by spatial GNNs. Using these tools, we analyze the inner workings of state of the art spatial architectures, in specific *aggregation-based* GNNs. We then propose a simple technique called *node masking* that helps these GNNs generalize and scale better. Finally, we empirically validate the theory by performing several experiments on two widely used benchmark datasets for node classification in both the transductive and inductive settings.

## 2. A brief history of GNNs

The concept of GNNs was first formalized in the work of Gori et al. (2005). The authors presented GNNs as an extension of *recursive neural networks* whereby they treat nodes as objects denoted by state vectors and edges as the relationships amongst those nodes. Their design consists of two main steps: i) iterative update of nodes’ state vectors based on the labels and state vectors of their neighbors up to a stable fixed point, and ii) back-propagation for adjustment

of parameters used in the update step. This approach was further refined in the work of Scarselli et al. (2009).

### 2.1. Spectral GNNs

Bruna et al. (2014) laid the foundation for generalization of the *convolution* operation from regular grids to graphs. Leveraging *spectral graph theory*, they proposed an architecture for performing *spectral convolutions* on graphs. Given a graph  $G$ , their architecture considers the feature vectors on nodes as multi-channel graph signals. It learns *spectral filters* that act on these signals in the *Fourier* domain defined by the eigenvectors of the *Laplacian* matrix of  $G$ . This architecture displays limited scalability since the filters learned are not localized, i.e., they act on the whole graph, and computation of the Laplacian’s eigenvectors is itself an expensive operation.

To overcome these issues, Defferrard et al. (2016) and Levie et al. (2017) proposed spectral architectures, *ChebNet* and *CayleyNet* respectively, comprising localized filters approximated by *Chebyshev* and *Cayley* polynomials. Kipf and Welling (2017) further simplified ChebNet by making the filters localized to 1-hop neighborhoods. By stacking multiple such filters in layers, they showed that any number of hops could be covered in the convolution operation. They called this new architecture *Graph Convolutional Network (GCN)*. Note that all spectral architectures are inherently transductive in that the filters learned on a graph are specific to the eigenbasis of its Laplacian. This not only limits the ability of these architectures to generalize to new nodes and edges. Although GCN itself is spectral, the idea of stacking multiple layers to cover higher-order neighborhoods led to the concept of spatial GNNs.

### 2.2. Spatial GNNs

Spatial GNNs define the convolution operation directly on the structure of the graph. In other words, they work by learning functions to compute representations for nodes or edges that capture the features and structures of their surrounding neighborhoods. Once learned, these functions can then be inductively applied to new nodes and edges. Spatial GNNs are preferred over their spectral counterparts due to their scalability, inductive capabilities, and ability to handle myriad types of graphs (Wu et al., 2019).

#### 2.2.1. SAMPLING-BASED

*GraphSAGE* (Hamilton et al., 2017) was one of the first spatial GNNs. For a node  $v$ , *GraphSAGE* randomly samples a fixed number of nodes from its  $K$ -hop neighborhood and learns to compute a representation for  $v$  based on its own features plus the features of its sampled neighbors. Note that this design does not exhibit *structural invariance*, i.e., the GNN cannot accommodate varying neighborhood structures

but rather constrains nodes to a fixed number of neighbors only. A clear drawback of such a sampling-based design is that a lot of neighborhood information is wasted.

### 2.2.2. AGGREGATION-BASED

Aggregation-based spatial GNNs eliminate the need for sampling fixed number of neighbors. They work by iteratively computing representations for nodes based on those of their respective neighbors. A  $k$ -layer aggregation-based GNN sequentially performs such updates  $k$  times, consequently computing a representation for every node that captures its  $k$ -hop neighborhood. The update operation performed by the  $k^{\text{th}}$  layer for a node  $v$  can be stated as:

$$h_v^{(k)} = f^{(k)} \left( h_v^{(k-1)}, g(\{h_u^{(k-1)} : u \in \mathcal{N}_v\}) \right) \quad (1)$$

where  $\mathcal{N}_v$  denotes the set of neighbors of  $v$ , and  $h_v^{(0)}$  is the input feature vector of  $v$ . The *aggregate* function  $g$  aggregates representations of neighbors, and the *combine* function  $f$  combines the aggregated representation with that of  $v$  itself. This formulation is general enough to cover the various aggregation-based GNNs that exist. All of them mainly differ in their choice of  $f$  and  $g$ .

Velickovic et al. (2018) proposed *Graph Attention Networks (GAT)* wherein a node’s representation is iteratively updated by aggregating the representations of its neighbors combining them with that of the node’s as per coefficients allocated by a *self-attention* mechanism. The defines the update operation in the  $k^{\text{th}}$  layer as:

$$h_v^{(k)} = \left\| \sigma \left( \sum_u^{v \cup \mathcal{N}_v} \alpha_l^{(k)}(v, u) \cdot W_l^{(k)} h_u^{(k-1)} \right) \right. \quad (2)$$

where  $\alpha_l^{(k)}(v, u)$  is the attention coefficient of node  $u$  with respect to node  $v$  from the  $l^{\text{th}}$  attention head,  $W_l$  is the weight matrix for the  $l^{\text{th}}$  attention head, and  $\|$  denotes concatenation across all the heads.

Xu et al. (2019) recently introduced the *Graph Isomorphism Network (GIN)* whose theoretical foundations allows it to be maximally powerful amongst the various spatial GNNs. The GIN- $\epsilon$  architecture defines the update operation as:

$$h_v^{(k)} = MLP^{(k)} \left( (1 + \epsilon^{(k)}) \cdot h_v^{(k-1)} + \sum_u^{\mathcal{N}_v} h_u^{(k-1)} \right) \quad (3)$$

where  $MLP$  represents a multi-layer perceptron.

In this paper, we focus on aggregation-based GNNs given that they yield state of the art (Wu et al., 2019) performance. We work with the GAT and GIN architectures only but our techniques can be applied to other aggregation-based GNNs.

## 3. Theoretical Framework

Hereon, we assume that the graphs we consider are undirected, implying that an edge can be traversed from either endpoints. That said, the work presented in this paper is trivially applicable to directed graphs too. We also assume that all nodes within a graph are uniquely identifiable.

### 3.1. Aggregation trees

We discuss the concept of *aggregation trees* as the theoretical tool for visualizing aggregation-based GNNs.

**Definition 1.** Given a graph  $G$  with a node  $v$  in it, let  $\mathcal{P}_v^k$  denote the set of all possible *walks* of length  $k$ , i.e., of  $k$  hops, starting at  $v$ . Walks are paths with possibly repeated nodes. The  $k$ -*aggregation tree*  $T_v^k$  of a node  $v$  is the smallest *arborescence* (Fournier, 2013) rooted at  $v$  such that  $w$  is a path from the root of  $T_v^k$  to a leaf in it if and only if  $w \in \mathcal{P}_v^k$ . Here, smallness is by the number of nodes. Note that  $T_v^k$  is of height  $k$  with all the leaves at the same depth. We refer to  $G$  itself as the *base graph* of  $T_v^k$ .

Aggregation trees have been explored in the past as graph kernels (Xu et al., 2019) under names like *tree-walks* (Bach, 2008) or *subtree patterns* (Shervashidze et al., 2011). Figure 3 shows an example of a graph along with the 2-aggregation tree of a node in it. Figure 4 shows other trees that have the same root node and the same set of paths from the root to leaves but are not valid 2-aggregation trees. We would like to point out to the reader that the two assumptions we made for graphs are not upheld in the case of aggregation trees:

- Aggregation trees can contain multiple replicas of the same node (Shervashidze et al., 2011). For example, the tree  $T_a^2$  shown in figure 3 has node  $a$  as the root and also as leaves. The replicas are treated as distinct nodes so that aggregation trees remain acyclic, but all of them correspond to the same node in the base graph.
- Aggregation trees are directed, making the notion of neighbor set different in their case than in the case of undirected graphs. In an aggregation tree, the neighbor set  $\mathcal{N}_v$  of a node  $v$  only contains those nodes that have incoming edges from  $v$ , but not those that have outgoing edges to  $v$ . Therefore, in the context of aggregation trees, we refer to the neighbor set of a node as its *set of children* or *child set* for clarity.

The lemmas below highlight two core properties of the trees.

**Lemma 1.** In a given  $k$ -aggregation tree  $T_v^k$ , a *subtree* is any node along with all its children up to some depth  $l$  ( $l \leq k$ ). Every *subtree* of  $T_v^k$  is also an aggregation tree.

*Proof.* If the subtree under some node  $u$  is not an aggregation tree, then there exists a path in  $T_v^k$  via  $u$  that is not a  $k$ -length walk in the base graph or vice versa; a contradiction.  $\square$

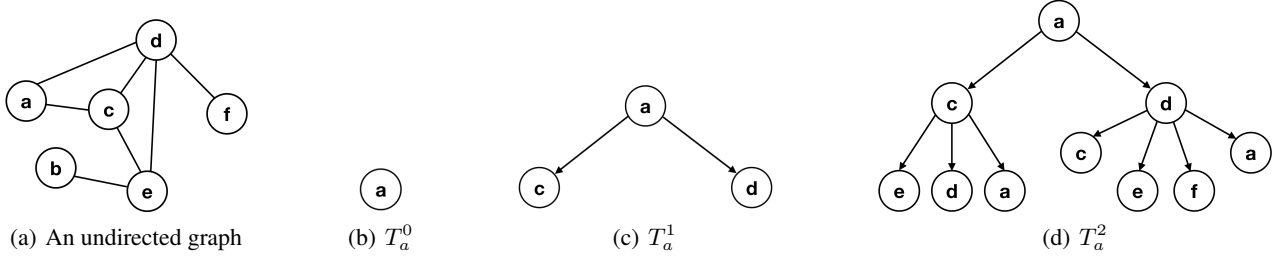


Figure 3. Sub-figure (a) shows an undirected graph, i.e., edges can be walked in either directions. Sub-figures (b-d) show some aggregation trees  $T_a^k$  of node  $a$ . Every path from the root of a  $T_a^k$  to some leaf in it is a valid  $k$ -hop walk in the graph starting at node  $a$ , and vice versa.

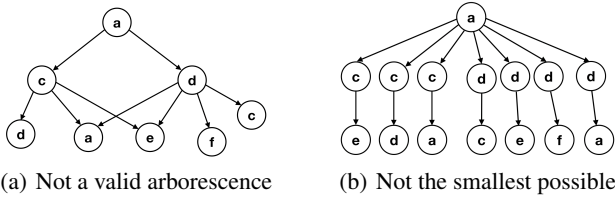


Figure 4. Trees having the required paths from the root to leaves, however, not the valid 2-aggregation tree of  $a$ . Sub-figure (a) is not a valid arborescence since there should only be one path from the root to any node in an arborescence (Gordon & McMahon, 1989).

**Lemma 2.** Given a graph  $G$ , let  $v$  be any node in it without loss of generality. The child set of any non-leaf node in  $T_v^k$  is equal to the neighbor set of its corresponding node in  $G$ .

*Proof.* We prove this also by contradiction. A non-leaf node in  $T_v^k$  must be reachable in  $k - 1$  hops from  $v$  in  $G$ . Then if there exists a non-leaf node in  $T_v^k$  such that its child set is not equal to its corresponding neighbor set in  $G$ , that would imply that there exists a path from the root of  $T_v^k$  to a leaf in it that is not a  $k$ -length walk in  $G$ , or vice versa. However, that would contradict the definition of  $k$ -aggregation trees. Hence such a non-leaf node cannot exist.  $\square$

### 3.2. Connection to aggregation-based GNNs

We now establish the connection between aggregation trees and aggregation-based GNNs.

**Theorem 1.** Given a graph  $G$ , let  $v$  be any node in it without loss of generality. The  $k$ -aggregation tree  $T_v^k$  of  $v$  denotes the structure captured by the representation  $h_v^{(k)}$  computed using a  $k$ -layer aggregation-based GNN for  $v$ . Alternatively, a  $k$ -layer aggregation-based GNN, when applied to  $T_v^k$ , computes the same representation  $h_v^{(k)}$  for root  $v$  as it does for node  $v$  when applied to  $G$ .

*Proof.* We prove this by induction on  $k$ . As per equation 1, when  $k = 1$ , the computation of  $h_v^{(1)}$  by a 1-layer aggregation-based GNN is given by:

$$h_v^{(1)} = f^{(1)} \left( h_v^{(0)}, g(\{h_u^{(0)} : u \in \mathcal{N}_v\}) \right)$$

By lemma 2, we have that the child set of root  $v$  in  $T_v^1$  is identical to the neighbor set of  $v$  in  $G$ . Furthermore,  $h_*^{(0)}$  are the input feature vectors for nodes; any node in  $T_v^1$  has the same  $h_*^{(0)}$  as its corresponding node in  $G$ . So, the theorem trivially holds for  $k = 1$ . Assume that the theorem also holds for some  $k > 1$ , i.e.,  $h_v^{(k)}$  computed for root  $v$  of  $T_v^k$  by a  $k$ -layer aggregation-based GNN is identical to  $h_v^{(k)}$  computed for node  $v$  in  $G$ . Now, the computation of  $h_v^{(k+1)}$  by a  $k + 1$ -layer aggregation-based GNN is given by:

$$h_v^{(k+1)} = f^{(k+1)} \left( h_v^{(k)}, g(\{h_u^{(k)} : u \in \mathcal{N}_v\}) \right)$$

As before, we have that the child set of root  $v$  in  $T_v^{k+1}$  is identical to the neighbor set of  $v$  in  $G$ . Additionally, the representations  $h_*^{(k)}$  for root  $v$  and its children capture the respective subtrees of depth  $k$  under them. Since, these subtrees are actually  $k$ -aggregation trees (lemma 1), following our assumption,  $h_*^{(k)}$  must be the same for root  $v$  and its children as for the corresponding nodes in  $G$ . So, the theorem holds for  $k + 1$  when it holds for  $k$  because inputs to the computation of  $h_v^{(k+1)}$  are the same in the case of  $T_v^{k+1}$  and  $G$ . Hence, the theorem holds for  $k \geq 1$ .  $\square$

So, the  $k$ -aggregation tree  $T_v^k$  is a visual depiction of the representation  $h_v^{(k)}$  computed by a  $k$ -layer aggregation-based GNN. Every subtree in  $T_v^k$  is the depiction of some representation  $h_*^{(l)}$  ( $l < k$ ) computed intermediately.

## 4. Analysis of aggregation-based GNNs

Aggregation trees surface two important issues stemming from the way that aggregation-based GNNs operate.

The first one concerns the *generalization* ability of these architectures. A  $k$ -layer aggregation-based GNN with  $k > 1$  can aggregate a node  $v$  multiple times when computing the representation  $h_v^{(k)}$ . An example of this can be seen in

figure 3 where the node  $a$  appears multiple times in its own 2-aggregation tree  $T_a^2$ . Such a repetition can easily bias the GNN in the training phase to focus on a node’s own features instead of fully leveraging the information present in its neighborhood. Moreover, due to repetition, the GNN can learn to simply associate together a node and its neighbors in the training graph, thus hurting the ability to generalize.

The second issue pertains to *scalability* of a  $k$ -layer aggregation-based GNN where  $k > 1$ . In many real-world settings, there is a large graph that keeps growing with time. A prime example is social networks where new users join from time to time. In such settings, learning follows the inductive paradigm whereby we train the GNN on a snapshot of the graph, and then predict on new nodes that enter the graph after that. Figure 5(a) depicts such a setting where  $v$  is a node entering the graph after training. Figure 5(b) shows the  $k$ -aggregation tree  $T_v^k$ , i.e., the structure that will be captured by the representation  $h_v^{(k)}$ . Essentially, the GNN requires input vectors  $h_*^{(0)}$  for all the nodes within  $k$  hops of  $v$  to compute  $h_v^{(k)}$ . This can be up to  $\mathcal{O}(d^k)$  representations in total, where  $d$  is the average degree of a node.

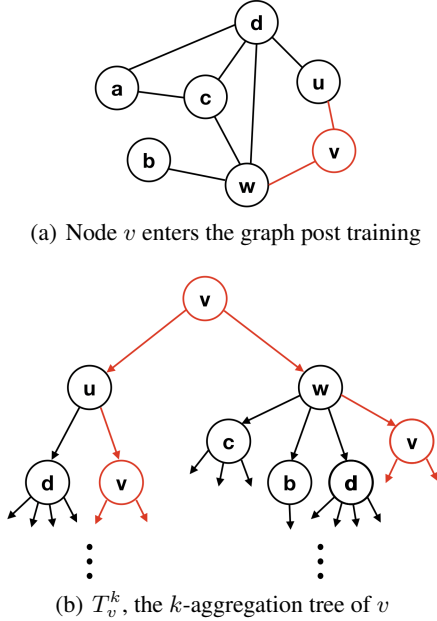


Figure 5. Depiction of the scenario where a node  $v$  enters a graph after training. The  $k$ -aggregation tree of node  $v$  is also shown.

Storing representations from layers of a GNN has been explored before (Chen et al., 2018) as an optimization technique. In the example above, the representations  $h_u^{(*)}$  and  $h_w^{(*)}$  can be *cached* at the end of training since they capture the relevant aggregation trees of  $u$  and  $w$  respectively. Then the representation  $\hat{h}_v^{(k)}$  can be approximated as:

$$\hat{h}_v^{(k)} = f^{(k)} \left( \hat{h}_v^{(k-1)}, g(\{\tilde{h}_u^{(k-1)} : u \in \mathcal{N}_v\}) \right) \quad (4)$$

where  $\tilde{h}$  denotes the cached representations, and  $\hat{h}$  signifies that the computed representation is an approximation of  $h_v^{(k)}$ . The  $k$ -aggregation tree for equation 4 is shown in figure 6. Note that, unlike 5(b), now  $v$  only appears as the root, making  $h_v^{(k)}$  and  $\hat{h}_v^{(k)}$  different. This is because  $v$  was not present during training, and consequently, not covered by the cached representations.

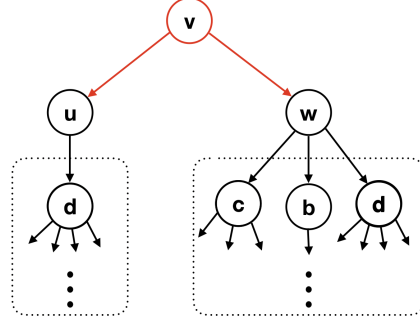


Figure 6. The  $k$ -aggregation tree of node  $v$  as per equation 4. The dotted boxes encapsulate the aggregation trees captured by cached representations  $\tilde{h}_*^{(1)}, \dots, \tilde{h}_*^{(k-1)}$  for  $u$  and  $w$ .

Essentially, with caching, the GNN only requires the  $k$  representations  $\tilde{h}_*^{(0)}, \dots, \tilde{h}_*^{(k-1)}$  for every neighbor of  $v$  in order to approximate  $h_v^{(k)}$ , i.e., up to  $\mathcal{O}(kd)$  representations in total. While this is a substantial gain in efficiency, we show empirically in section 6 that the performance at prediction suffers given that the structure of aggregation trees differs between training and prediction times.

## 5. Node Masking

We propose *node masking* as a novel yet simple training phase technique to alleviate the issues highlighted in the previous section. We begin by formalizing the notion of a *masking function* for generic countable sets.

**Definition 2.** Let  $\mathcal{S}$  be a set of elements; we assume  $\mathcal{S}$  is countable. Let  $\mathcal{B}_p^n$  be the set of outputs of  $n$  Bernoulli trials ( $n = |\mathcal{S}|$ ) with probability  $p$  of success. We define  $\delta_p$  to be a bijective mapping from  $\mathcal{S}$  to  $\mathcal{B}_p^n$ , and refer to it as the *Bernoulli select function*. There can be  $n!$  different  $\delta_p$ . Now, the *masking function*  $\mathcal{M}$  can be defined for  $\mathcal{S}$  and a  $\delta_p$  as:

$$\mathcal{M}(\mathcal{S}, \delta_p) = \{e : e \in \mathcal{S}, \delta_p(e) = 1\} \quad (5)$$

Here, all the elements  $e$  with  $\delta_p(e) = 0$  are said to be *masked*. Next, we demonstrate how we inculcate this masking function  $\mathcal{M}$  in the computations of aggregation-based GNNs to tackle the issues we discussed in the previous section. Let  $\delta_p^G$  be the Bernoulli select function over the set of nodes of a given graph  $G$ . We propose *node masking* as the following modification to equation 1 that defines the update

operation in the  $k^{\text{th}}$  layer of an aggregation-based GNN:

$$h_v^{(k)} = f^{(k)}\left(h_v^{(k-1)}, g\left(\{h_u^{(k-1)} : u \in \mathcal{M}(\mathcal{N}_v, \delta_p^G)\}\right)\right) \quad (6)$$

We refer to  $p$  as the *node masking rate*. If  $p$  is set to 1 in  $\delta_p^G$ , then equation 6 resembles equation 1, i.e., node masking has no effect. Thus, we say node masking is *inactive* when  $p = 1$  and *active* when  $p < 1$ .

The actual implementation of node masking may vary across the different aggregation-based GNNs. Equations 7 and 8 lay out the implementations of node masking in GAT and GIN-0 (Xu et al., 2019) architectures respectively.

$$h_v^{(k)} = MLP^{(k)}\left(h_v^{(k-1)} + \sum_u \delta_p^G(u) \cdot h_u^{(k-1)}\right) \quad (7)$$

$$h_v^{(k)} = \left\| \sigma\left(\sum_u \delta_p^G(u) \cdot \alpha_l^{(k)}(v, u) \cdot W_l^{(k)} h_u^{(k-1)}\right)\right\|_l \quad (8)$$

In both cases, any node  $u$  with  $\delta_p^G(u) = 0$  is effectively masked since its contribution to the sum is nullified.

Essentially, given a graph  $G$  and a  $k$ -layer aggregation-based GNN, if a node  $v$  in  $G$  is masked, then the representations  $h_v^{(l)}$  ( $l < k$ ) are discarded during the computations performed by the GNN. The equivalent effect in aggregation trees is that  $v$  is not included in the child set of other nodes in any aggregation tree since it cannot contribute to representations of other nodes. Going back to the example graph in figure 3, figure 7 shows some possible 2-aggregation trees  $T_a^2$  of the node  $a$  in it depending on nodes that are masked. Note that even if a node is masked, it still appears as the root of its own aggregation trees.

When a  $k$ -layer aggregation-based GNN with active node masking is trained on some graph  $G$ , a Bernoulli select function  $\delta_p^G$  is randomly sampled in every training epoch, allowing the GNN to see many different  $T_v^k$  for every node  $v$ . This has two advantages. First, the GNN is discouraged from simply associating a node and its neighbors together. Second, if  $\delta_p^G(v) = 0$  in an epoch, then  $T_v^k$  has the same structure as the aggregation tree in figure 6, i.e., no repetition of  $v$  in  $T_v^k$ . This reduces the tendency of the GNN to focus heavily on  $v$ 's own features and also sensitizes the GNN to that structure of aggregation trees that it may capture at prediction time if caching is used.

In summary, node masking can be seen a *data augmentation* technique for training phase that stresses the relational inductive biases, while also having a regularizing effect that prevents aggregation-based GNNs from easily memorizing associations amongst features and neighborhoods in the training graph. Once training has finished, node masking is easily inactivated by setting the node masking rate  $p$  to 1.

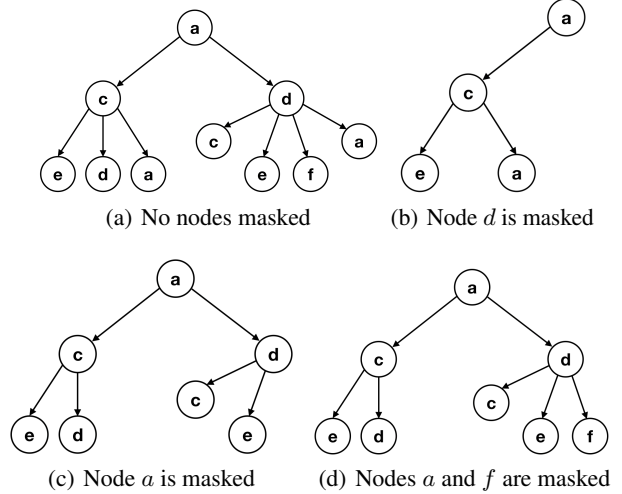


Figure 7. Some possible 2-aggregation trees  $T_a^2$  of node  $a$  in the base graph shown by figure 3(a). The aggregation trees vary based on the nodes that are masked. If a node is masked, it is excluded from the child set of other nodes but can still appear as the root.

## 6. Experiments

To empirically verify the theory we have discussed up till now, we conduct over 100 experiments, covering both the aspects we highlighted, i.e., generalization and scalability.

### 6.1. Datasets

We work with two widely-used benchmark datasets for node classification, namely *Cora* and *PubMed* citation networks (Sen et al., 2008).

**Cora.** The *Cora* citation network dataset consists of 2,708 nodes and 5,429 edges. Nodes denote scientific publications and edges denote the citation relationships amongst them. Note that the edges are undirected for the purpose of the dataset even though citations are not symmetric (Kipf & Welling, 2017; Veličković et al., 2018). The publications are represented as binary bag-of-words feature vectors consisting of 1433 features each. Every node belongs to one of the seven classes, indicating the area of publication, e.g., *Genetic Algorithms* or *Reinforcement Learning*.

**PubMed.** The *PubMed diabetes* dataset consists of 19,717 nodes and 44,338 edges. Nodes denote scientific publications on diabetes and edges denote the citation relationships amongst them. As before, the edges are undirected for the purpose of the dataset even though citations are not symmetric. The publications are represented as *TF-IDF* weighted bag-of-words feature vectors consisting of 500 features each. Every node belongs to one of the three classes, indicating the type of diabetes that the publication pertains to, e.g., *Diabetes Mellitus Type 1* or *Diabetes Mellitus Type 2*.

## 6.2. Models and configurations

We experiment with both of the aggregation-based GNNs that we have discussed up till now, i.e., GAT and GIN. For the GIN architecture, we utilize the formulation specified by equation 7. If node masking is inactive, this formulation behaves exactly like the GIN-0 architecture from the original paper (Xu et al., 2019) that was shown to have state of the art performance. For the GAT architecture, we use the original formulation (Veličković et al., 2018) specified by equation 2. Additionally, we define a variant of GAT that we refer to as *simple* GAT or *SGAT*:

$$h_v^{(k)} = \left\| \sigma \left( \sum_u \frac{\delta_p^G(u)}{|v \cup \mathcal{N}_v|} \cdot W_l^{(k)} h_u^{(k-1)} \right) \right\|_l \quad (9)$$

When node masking is inactive, this variant behaves exactly like the original GAT architecture except that the attention coefficients are now simply the inverse of a node’s degree. In the GAT paper, the authors apply dropout on the attention coefficients in order to stochastically sub-sample neighborhoods of nodes by randomly dropping edges. They do so to make the learning process more robust to over-fitting. Dropout can likewise be used on coefficients in SGAT, provided that node masking is kept inactive. The concept of randomly discarding edges has also been explored in spectral GNNs under the name *DropEdge* (Rong et al., 2020) to alleviate over-fitting and over-smoothing.

## 6.3. Experimental settings

We use *PyTorch* (Paszke et al., 2019) for modeling. For the GAT and SGAT architectures, we set the exact same hyper-parameters as in the original paper (Veličković et al., 2018) for the *Cora* dataset. We do not experiment with GAT and SGAT on the *PubMed* dataset because that requires support for operations like *sparse softmax* (Veličković et al., 2018), which are not available in *PyTorch* yet. Akin to GAT, we found a 2-layer GIN to be optimal for both the datasets. We set the maximum number of epochs to 500 with an early stopping patience of 50 epochs. We use the *Adam* optimizer (Kingma & Ba, 2015) to update the parameters. If node masking is active, then in every training epoch, we randomly sample a Bernoulli select function over the nodes in the train set. Node masking is always inactive outside training.

We experiment with both transductive and inductive learning paradigms. In the transductive setting, we make the entire graph from the dataset available at training time, i.e., all the nodes and edges. That said, the the loss for back-propagation is calculated using labels on the nodes in the train set only. In the inductive setting, we only make available at training time the graph  $\mathcal{G}$  formed by nodes in the train set plus the edges amongst them. At validation and test

times, we introduce the relevant nodes from the dataset into  $\mathcal{G}$  along with the relevant edges.

In both transductive and inductive settings, we experiment with multiple splits of the two datasets. Specifically, for each dataset, we experiment with 10%, 20%, 25%, 33%, 50%, 75%, and 90% of the nodes as the train set. In all the cases, the remaining data forms our test set except for a small part that is designated as the validation set for evaluation of the early stopping criterion in the training phase. For every split, we perform stratified partitioning of the data to ensure similar class distribution. Note that the metrics we present from our experiments are all in fact mean metrics over 10 trials with random initialization of the parameters.

## 6.4. Generalization

To show that node masking helps aggregation-based GNNs generalize better, we compare the performances yielded by the models when node masking is active versus when it is inactive. We denote the configurations where node masking is active by “+NM” and use a consistent rate of  $p = 0.5$ . That said,  $p$  is a hyper-parameter that can be tuned for further gains; figures 8 and 9 in appendix A explore the change in performance as  $p$  varies.

Table 1. Macro  $F_1$  scores on the *Cora* dataset in inductive and transductive settings for various sizes  $s$  of the train set (in percentage). Numbers in bold are significantly better than their counterparts with  $P$ -value  $< 0.05$  under paired  $t$ -test.

	$s$	GAT	SGAT	SGAT+NM
Inductive	10	40.74	40.57	<b>50.64</b>
	20	68.40	68.50	<b>74.82</b>
	25	74.12	74.34	<b>79.32</b>
	33	80.44	80.30	<b>82.74</b>
	50	84.77	85.04	<b>85.44</b>
	75	87.20	87.16	87.07
	90	86.86	86.46	86.94
Transductive	10	82.01	82.17	<b>83.46</b>
	20	84.20	84.35	<b>85.34</b>
	25	84.95	85.12	<b>85.88</b>
	33	85.87	85.86	<b>86.72</b>
	50	87.29	87.32	<b>87.61</b>
	75	88.38	88.43	88.44
	90	87.25	87.24	87.22

Table 1 shows the results for GAT, SGAT and SGAT+NM on the *Cora* dataset. Note that in SGAT+NM, we do not use any dropout on the attention coefficients. SGAT+NM outperforms both GAT and SGAT across several splits in both transductive and inductive settings. The gains are more pronounced in the inductive setting and amongst smaller sizes of the train set. Even though SGAT+NM simply uses inverse of nodes’ degrees as attention coefficients, it is able to improve over the more computationally intensive GAT.

Moreover, the wins over SGAT indicate that node masking is more effective than simply dropping edges to sub-sample since the latter does not address the issue of repetition of nodes in aggregation trees.

Tables 2 and 3 show the results for GIN versus GIN+NM on the *Cora* and *PubMed* datasets respectively. Again, node masking helps boost performance across almost all splits in both transductive and inductive settings.

Table 2. Macro  $F_1$  scores on the *Cora* dataset in inductive and transductive settings for various sizes  $s$  of the train set (in percentage). Numbers in bold are significantly better than their counterparts with  $P$ -value  $< 0.05$  under paired  $t$ -test.

$s$	Inductive		Transductive	
	GIN	GIN+NM	GIN	GIN+NM
10	52.91	<b>56.38</b>	77.95	<b>79.65</b>
20	71.10	<b>74.38</b>	81.65	<b>82.66</b>
25	74.71	<b>77.94</b>	82.72	<b>83.87</b>
33	78.84	<b>80.98</b>	83.78	<b>84.61</b>
50	83.07	<b>84.49</b>	85.63	<b>86.57</b>
75	85.46	<b>86.88</b>	87.94	87.91
90	85.13	<b>86.63</b>	86.67	<b>87.82</b>

Table 3. Macro  $F_1$  scores on the *PubMed* dataset in inductive and transductive settings for various sizes  $s$  of the train set (in percentage). Numbers in bold are significantly better than their counterparts with  $P$ -value  $< 0.05$  under paired  $t$ -test.

$s$	Inductive		Transductive	
	GIN	GIN+NM	GIN	GIN+NM
10	77.51	<b>78.31</b>	83.65	<b>84.34</b>
20	82.11	<b>82.86</b>	84.61	<b>85.20</b>
25	82.95	<b>83.94</b>	85.03	<b>85.47</b>
33	83.78	<b>84.46</b>	85.35	<b>85.84</b>
50	85.25	<b>85.79</b>	85.89	<b>86.42</b>
75	85.99	<b>86.53</b>	86.38	86.55
90	86.42	<b>86.80</b>	86.43	86.47

### 6.5. Scalability

Tables 4 and 5 compare performances of the GIN-0 model on the *Cora* and *PubMed* datasets respectively when caching is used versus when it is not. For both settings, the tables also indicate the number of unique nodes involved in the computations done by the model at the time of prediction. We note that gains in efficiency from caching are more pronounced when the training graph is significantly larger than the set of nodes and edges entering at prediction time, a common scenario in the real-world. However, as stated before, the model performs worse with caching because the structure of aggregation trees it captures at prediction time differs from the structure it learned to capture at training time. That

said, when node masking is used, the performance in fact exceeds the configuration without caching.

Table 4. Macro  $F_1$  scores on the *Cora* dataset in inductive setting with and without caching for various sizes  $s$  of the train set (in percentage).  $F_1$  scores in bold are significantly better than their counterparts with  $P$ -value  $< 0.05$  under paired  $t$ -test.

$s$	GIN		GIN + Caching		
	$F_1$	# NODES	$F_1$	$F_1$ (+NM)	# NODES
10	52.91	2708	51.89	<b>55.82</b>	<b>2698</b>
20	71.10	2708	69.59	<b>74.17</b>	<b>2672</b>
25	74.71	2708	73.55	<b>77.32</b>	<b>2644</b>
33	78.84	2708	77.60	<b>80.72</b>	<b>2605</b>
50	83.07	2708	82.50	<b>83.95</b>	<b>2426</b>
75	85.46	2708	84.90	<b>86.59</b>	<b>1781</b>
90	85.13	2708	84.81	<b>85.85</b>	<b>919</b>

Table 5. Macro  $F_1$  scores on the *PubMed* dataset in inductive setting with and without caching for various sizes  $s$  of the train set (in percentage).  $F_1$  scores in bold are significantly better than their counterparts with  $P$ -value  $< 0.05$  under paired  $t$ -test.

$s$	GIN		GIN + Caching		
	$F_1$	# NODES	$F_1$	$F_1$ (+NM)	# NODES
10	77.51	19717	76.25	<b>78.33</b>	<b>19614</b>
20	82.11	19717	81.47	<b>82.75</b>	<b>19300</b>
25	82.95	19717	82.24	<b>83.77</b>	<b>19059</b>
33	83.78	19717	82.83	<b>84.15</b>	<b>18553</b>
50	85.25	19717	84.27	<b>85.34</b>	<b>16733</b>
75	85.99	19717	85.46	<b>86.01</b>	<b>11944</b>
90	86.42	19717	85.87	<b>86.61</b>	<b>6682</b>

## 7. Conclusion

In this paper, we introduced *node masking*, a novel concept that significantly improves the performance of state of the art graph neural networks (GNNs). We first discussed some theoretical tools to better visualize the operations performed by spatial aggregation-based GNNs. Using these tools, we highlighted the issues that limit the ability of such GNNs to generalize and scale. Finally, we empirically demonstrated the effectiveness of node masking in enhancing performance of aggregation-based GNNs on two widely-used benchmark datasets for node classification, *PubMed* and *Cora* citation network.

## References

- Bach, F. R. Graph kernels between point clouds. In *Proceedings of the 25th International Conference on Machine Learning, ICML 08*, pp. 2532, New York, NY, USA, 2008. Association for Computing Machinery. ISBN 9781605582054. doi: 10.1145/1390156.



1390160. URL <https://doi.org/10.1145/1390156.1390160>.
- Battaglia, P. W., Hamrick, J. B., Bapst, V., Sanchez-Gonzalez, A., Zambaldi, V. F., Malinowski, M., Tacchetti, A., Raposo, D., Santoro, A., Faulkner, R., Gülçehre, Ç., Song, H. F., Ballard, A. J., Gilmer, J., Dahl, G. E., Vaswani, A., Allen, K. R., Nash, C., Langston, V., Dyer, C., Heess, N., Wierstra, D., Kohli, P., Botvinick, M., Vinyals, O., Li, Y., and Pascanu, R. Relational inductive biases, deep learning, and graph networks. *CoRR*, abs/1806.01261, 2018. URL <http://arxiv.org/abs/1806.01261>.
- Bruna, J., Zaremba, W., Szlam, A., and LeCun, Y. Spectral networks and locally connected networks on graphs. In *Proceedings of The International Conference on Learning Representations*, 2014.
- Chen, J., Zhu, J., and Song, L. Stochastic training of graph convolutional networks with variance reduction. In *International Conference on Machine Learning*, pp. 941–949, 2018.
- Chiang, W.-L., Liu, X., Si, S., Li, Y., Bengio, S., and Hsieh, C.-J. Cluster-gcn: An efficient algorithm for training deep and large graph convolutional networks. In *ACM SIGKDD Conference on Knowledge Discovery and Data Mining (KDD)*, 2019. URL <https://arxiv.org/pdf/1905.07953.pdf>.
- Defferrard, M., Bresson, X., and Vandergheynst, P. Convolutional neural networks on graphs with fast localized spectral filtering. In *NIPS*, pp. 3844–3852, 2016.
- Fournier, J.-C. *Graphs theory and applications: with exercises and problems*. John Wiley & Sons, 2013.
- Gordon, G. and McMahon, E. A greedoid polynomial which distinguishes rooted arborescences. *Proceedings of the American Mathematical Society*, 107(2):287–298, 1989.
- Gori, M., Monfardini, G., and Scarselli, F. A new model for learning in graph domains. In *Proceedings. 2005 IEEE International Joint Conference on Neural Networks, 2005.*, volume 2, pp. 729–734 vol. 2, July 2005. doi: 10.1109/IJCNN.2005.1555942.
- Hamilton, W., Ying, Z., and Leskovec, J. Inductive representation learning on large graphs. In *Advances in Neural Information Processing Systems*, pp. 1024–1034, 2017.
- Kingma, D. P. and Ba, J. Adam: A method for stochastic optimization. In *Proceedings of the 3rd International Conference on Learning Representations, ICLR '15*, 2015.
- Kipf, T. N. and Welling, M. Semi-supervised classification with graph convolutional networks. In *Proceedings of the 5th International Conference on Learning Representations, ICLR '17*, 2017. URL <https://arxiv.org/pdf/1609.02907.pdf>.
- Lake, B. M. and Baroni, M. Still not systematic after all these years: On the compositional skills of sequence-to-sequence recurrent networks. In *Proceedings of the 3rd International Conference on Learning Representations*, 2017. URL <https://openreview.net/pdf?id=H18WqugAb>.
- Levie, R., Monti, F., Bresson, X., and Bronstein, M. M. Cayleynets: Graph convolutional neural networks with complex rational spectral filters. *IEEE Transactions on Signal Processing*, 67(1):97–109, 2017.
- Mishra, P., Del Tredici, M., Yannakoudakis, H., and Shutova, E. Abusive language detection with graph convolutional networks. In *Proceedings of the 2019 Conference of the North American Chapter of the Association for Computational Linguistics: Human Language Technologies*. Association for Computational Linguistics, 2019. URL <https://arxiv.org/abs/1904.04073>.
- Paszke, A., Gross, S., Massa, F., Lerer, A., Bradbury, J., Chanan, G., Killeen, T., Lin, Z., Gimelshein, N., Antiga, L., Desmaison, A., Kopf, A., Yang, E., DeVito, Z., Raison, M., Tejani, A., Chilamkurthy, S., Steiner, B., Fang, L., Bai, J., and Chintala, S. Pytorch: An imperative style, high-performance deep learning library. In Wallach, H., Larochelle, H., Beygelzimer, A., d'Alché-Buc, F., Fox, E., and Garnett, R. (eds.), *Advances in Neural Information Processing Systems 32*, pp. 8024–8035. Curran Associates, Inc., 2019. URL <https://arxiv.org/abs/1912.01703>.
- Rong, Y., Huang, W., Xu, T., and Huang, J. Dropedge: Towards deep graph convolutional networks on node classification. In *International Conference on Learning Representations*, 2020. URL <https://openreview.net/forum?id=Hkx1qkrKPr>.
- Sahu, S. K., Christopoulou, F., Miwa, M., and Ananiadou, S. Inter-sentence relation extraction with document-level graph convolutional neural network. In *Proceedings of the 57th Annual Meeting of the Association for Computational Linguistics*, pp. 4309–4316, Florence, Italy, July 2019. Association for Computational Linguistics. doi: 10.18653/v1/P19-1423. URL <https://www.aclweb.org/anthology/P19-1423>.
- Scarselli, F., Gori, M., Tsoi, A. C., Hagenbuchner, M., and Monfardini, G. The graph neural network model. *IEEE Transactions on Neural Networks*, 20(1):61–80, Jan 2009. doi: 10.1109/TNN.2008.2005605.

- Sen, P., Namata, G., Bilgic, M., Getoor, L., Galligher, B., and Eliassi-Rad, T. Collective classification in network data. *AI Magazine*, 29(3):93, Sep. 2008. doi: 10.1609/aimag.v29i3.2157. URL <https://www.aaai.org/ojs/index.php/aimagazine/article/view/2157>.
- Shervashidze, N., Schweitzer, P., van Leeuwen, E. J., Mehlhorn, K., and Borgwardt, K. M. Weisfeiler-lehman graph kernels. *J. Mach. Learn. Res.*, 12(null):25392561, November 2011. ISSN 1532-4435.
- Tenenbaum, J. B., Kemp, C., Griffiths, T. L., and Goodman, N. D. How to grow a mind: Statistics, structure, and abstraction. *science*, 331(6022):1279–1285, 2011.
- Veličković, P., Cucurull, G., Casanova, A., Romero, A., Liò, P., and Bengio, Y. Graph Attention Networks. In *International Conference on Learning Representations*, 2018. URL <https://openreview.net/forum?id=rJXMpikCZ>. accepted as poster.
- Wang, Z., Lv, Q., Lan, X., and Zhang, Y. Cross-lingual knowledge graph alignment via graph convolutional networks. In *Proceedings of the 2018 Conference on Empirical Methods in Natural Language Processing*, pp. 349–357, Brussels, Belgium, October–November 2018. Association for Computational Linguistics. doi: 10.18653/v1/D18-1032. URL <https://www.aclweb.org/anthology/D18-1032>.
- Wu, Z., Pan, S., Chen, F., Long, G., Zhang, C., and Yu, P. S. A comprehensive survey on graph neural networks. *CoRR*, abs/1901.00596, 2019. URL <http://arxiv.org/abs/1901.00596>.
- Xu, K., Hu, W., Leskovec, J., and Jegelka, S. How powerful are graph neural networks? In *International Conference on Learning Representations*, 2019. URL <https://openreview.net/forum?id=ryGs6iA5Km>.

## A. Varying the node masking rate

Figures 8 and 9 explore the change in performance for increasing  $p$ , from 0 (i.e. inactive node masking) up to  $p = 0.95$ , across multiple setups, demonstrating how the node masking rate fine-tuning can be leveraged to obtain further gains. For example, as seen in figure 8, the performance of GIN on the Cora dataset in inductive setting peaks for  $p > 0.5$  for all three data splits considered.

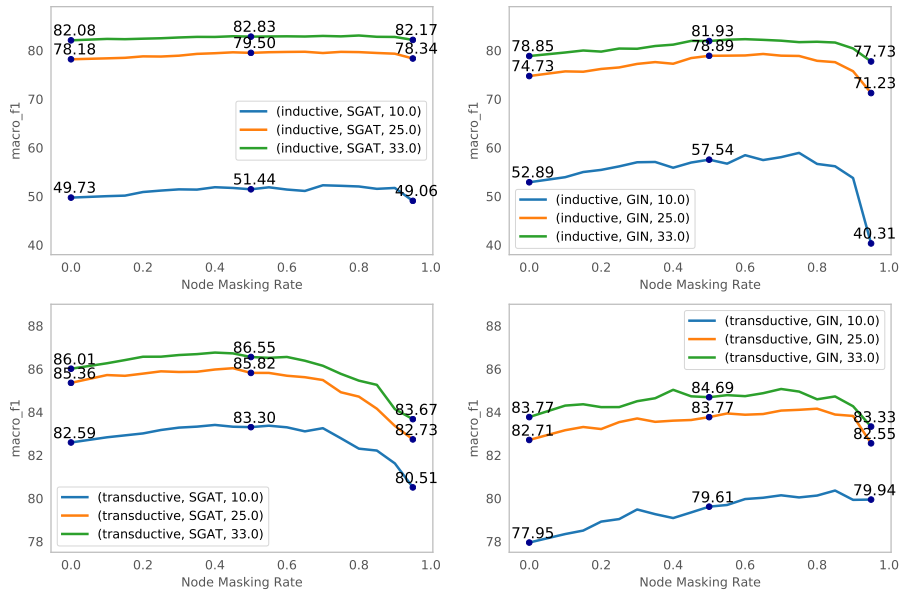


Figure 8. Results on the *Cora* dataset for node masking rates  $p \in [0.0, 0.95]$ ; the  $y$ -axis denotes the macro F1 scores. We highlight results for  $p \in \{0.0, 0.5, 0.95\}$ . See plot legends for details of each setup in terms of the paradigm, model and train set size.

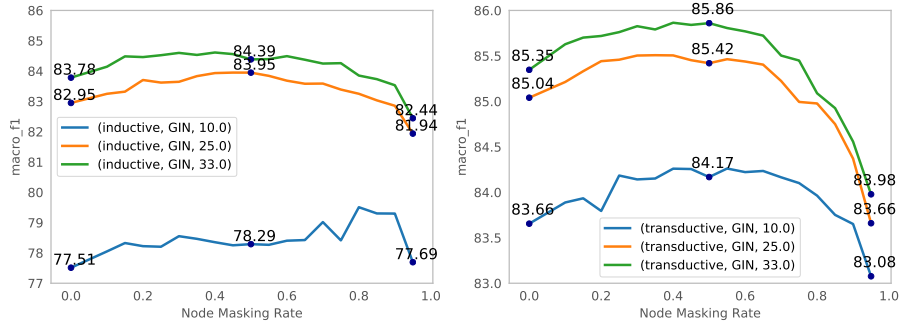


Figure 9. Results on the *PubMed* dataset for node masking rates  $p \in [0.0, 0.95]$ ;  $y$ -axis denotes the macro F1 scores. We highlight results for  $p \in \{0.0, 0.5, 0.95\}$ . See plot legends for details of each setup in terms of the paradigm, model and train set size.